American Mineralogist, Volume 90, pages 115–121, 2005

Ca_2SiO_3OHF—A high-pressure phase with dense calcium polyhedral packing and tetrahedral silicon

KURT LEINENWEBER,[1,2,*] JENNIFER E. JOHNSON,[1,2] AND THOMAS L. GROY[1]

[1]Department of Chemistry, Arizona State University, Tempe, Arizona 85287-1604, U.S.A.
[2]Department of Geology, Arizona State University, Tempe, Arizona 85287-1604, U.S.A.

ABSTRACT

The composition and structure of a new phase crystallizing in high-pressure experiments in the system CaO-$Ca(OH)_2$-CaF_2-SiO_2 are described. The composition is on the join $Ca_2SiO_3(OH)_2$-$Ca_2SiO_3F_2$, with the relative amounts of OH and F near 50/50 from electron probe microanalysis, or near the ideal midpoint composition Ca_2SiO_3OHF. The symmetry is monoclinic, space group $P2_1/c$, with a = 5.8111(7), b = 10.6050(13), and c = 6.6968(8) Å, and β = 102.025(3)°, V = 403.65(8) Å^3, Z = 4. In the structure isolated SiO_3OH tetrahedral groups occupy narrow linear channels whose axes lie along **a**. The channels are lined by two types of eight-coordinated CaO_5OHF_2 polyhedra that share edges and faces. The axes of the channels lie on a nearly hexagonal array in the **b**-**c** plane, leading to a c_p/b ratio of 0.618, close to the ideal ratio of 0.577 for a hexagonal array. However, there is no simple packing rule for either the cation or anion array. Although the channels are arranged in a nearly hexagonal fashion, the overall symmetry of the structure is not hexagonal, but instead has 5-rings of calcium polyhedra around the channels. The calcium atoms lie on a 5-3-5-3 net of triangles and pentagons that can be compared to the α-U_3O_8 net.

INTRODUCTION

The calcium silicates exhibit complex structural behavior, with a variety of structures occurring at ambient and high pressures in the compositions Ca_3SiO_5, Ca_2SiO_4, $Ca_3Si_2O_7$, and $CaSiO_3$. The tendency for unusual structural behavior in these compounds is well documented. One example is $CaSiO_3$ perovskite, a high-pressure phase that spontaneously converts to an amorphous phase while pressure is being released (Ringwood and Major 1971). A second example is high-pressure $CaSi_2O_5$ titanite, which develops five-coordinated silicon during pressure release under nonhydrostatic stress, the first documented example of this arrangement in a crystalline solid (Angel et al. 1996; Angel 1997; Stebbins and Poe 1999).

The addition of monovalent anions such as OH^- and F^- to the calcium silicate system allows additional structural flexibility. The system CaO-SiO_2-H_2O, for example, has silicate compounds with at least 25 distinct compositions (from the ICSD database; cf. Fluck 1996) stable at ambient pressure. Many new phases were also uncovered in an exploratory study of the system CaO-SiO_2-$CaCl_2$ by Stade at al. (1998). The monovalent anions significantly change the structural behavior of silicates because they have lower coordination and/or weaker bonds to metals, requiring only half as much total bond valence in order to be saturated. This modifies the structural networks, reducing the polymerization of the structure, and leaving voids, channels, etc. At the same time, the coordination numbers of the cations tend to increase when monovalent anions are added to a silicate, simply because there are more anions present in the structure. Given the interesting structures found in the CaO-SiO_2 system, new structural behavior can be anticipated when monovalent anions are added to this system and pressure is used as a variable. For example, new examples of pentacoordinate silicon could potentially be found in this system, as they are in the silica zeolites grown with fluorine, which form SiO_4F polyhedra (Koller et al. 1999).

Among the many already known examples of mixed-anion phases containing calcium and silicon and occurring at ambient pressure are structures such as cuspidine [$Ca_4Si_2O_7(F,OH)_2$] (Saburi et al. 1977), and various cement minerals such as α and β-$Ca_2SiO_3(OH)_2$ (Yano et al. 1993; Marsh 1994; Dai and Post 1995; Xu and Buseck 1996). The majority of these, because of their low structural density, are not likely high-pressure phases. In order to shed light on the effect of pressure on these compositions, high-pressure structural studies in the system Ca-Si-O-OH-F are being pursued. Exploratory work in the CaO-SiO_2-CaF_2-$Ca(OH)_2$ system has resulted in the growth of crystals with compositions near Ca_2SiO_3OHF.

EXPERIMENTAL METHODS

The unknown compound was encountered during a series of experiments on compositions containing $Ca(OH)_2$, CaF_2, and SiO_2 in various proportions and at various pressures and temperatures. A list of the pertinent high-pressure experiments is shown in Table 1.

Reagent grade CaF_2 (Fisher) and SiO_2 (SPEX Industries, Inc.) were used as purchased. In order to avoid the common problem of contamination by CO_2, fresh batches of $Ca(OH)_2$ were made by treating CaO [made by calcining $CaCO_3$ (Baker) at 960 °C and quenching in the absence of CO_2] in boiling water. This technique has been found in the past by Raman spectroscopic analysis, which is very sensitive to the presence of CO_3 groups, to result in samples of $Ca(OH)_2$ with no detectible $CaCO_3$ impurity. The starting materials were mixed by grinding under ethanol in an agate mortar and pestle.

For each high-pressure experiment, about 25 mg of starting material was placed in a platinum capsule 3.5 mm in diameter and 0.13 mm thick, and the capsule was welded at both ends using "trash can lids" made from 0.13 mm platinum foil (Holloway et al. 1992). The pressure, thermocouple temperature, and duration

* E-mail: kurtl@asu.edu

0003-004X/05/0001–115$05.00/DOI: 10.2138/am.2005.1528

TABLE 1. Summary of multianvil experiments relevant to the current study

Number	Starting	Pressure, temperature, time	Results
R-347	1	9.3 GPa, 1100 °C (est.), 15.5 hours	CSF + eF; ol; g
R-352	2	8.7 GPa, 1200 °C, 24.0 hours	unk; eF+F; g
R-353	1	9.3 GPa, 1100 °C, 4 days	ol+F; g, v
R-355	3	8.7 GPa, 1200 °C, 28 hours	hpF
R-369	4a	8.7 GPa, 1100 °C, 48 hours	ol, g
R-379	4b	8.7 GPa, 1100 °C, 25 hours	F + wal
R-381	4b	8.7 GPa, 1300 °C, 3.5 hours	F + wal
R-396	5	7.5 GPa, 900 °C, 24 hours	CSF + wal

Notes: The run products are listed in layers with increasing temperature, separated by semicolons, when layering is present. est = Temperature estimated from power relation. Starting materials: 1 = $Ca(OH)_2$ + $CaSiO_3$ + CaF_2; 2 = CaF_2 + SiO_2 + $Ca(OH)_2$; 3 = $Ca(OH)_2$ + CaF_2; 4a = $Ca(OH)_2$ + $CaSiO_3$; 4b = CaF_2 + $CaSiO_3$; 5 = $2CaSiO_3$ + $Ca(OH)_2$ + CaF_2. Products: CSF = Ca_2SiO_3OHF; eF = expanded fluorite (*a* can range from 5.470 to 5.486 Å); ol = Ca_2SiO_4 olivine phase (can be a quench derivative product of the larnite phase); g = glass; unk = unknown beam-sensitive CaSi phase; F = fluorite (*a* = 5.463 Å); hpF = CaF_2 in the $PbCl_2$ structure (Morris et al. 2001); v = vapor; wal = walstromite-type $CaSiO_3$.

are shown in Table 1. The materials were treated under pressure using pre-cast ceramic octahedra (Aremco 502-1550, Walker 1991) and a 6–8 multi-anvil pressure device with tungsten carbide cubes truncated to 8 mm edge lengths. A graphite box furnace (type "G2," Leinenweber and Parise 1995) was used to heat the sample, and a Type S thermocouple (Pt/Pt 10% Rh) was placed axially just outside one end of the cylindrical capsule, to measure the temperature as close to the sample as possible without puncturing the capsule.

The experiment that yielded the single crystals of the new phase, R-347, was at a pressure of 9.3 GPa. The crystals were found in the low-temperature part of the capsule (Fig. 1), coexisting with "expanded" CaF_2 fluorite (*a* = 5.486 Å, indicating about 8 mol% substitution of OH for F assuming Vegard's Law). The intermediate temperature part of the capsule was occupied by a layer of Ca_2SiO_4 olivine, and the high-temperature part by a glass. Because the thermocouple was not working in that experiment, the temperature (1100 °C) was estimated from the power supplied to the furnace. A subsequent experiment, R-396, was run at a pressure of 7.5 GPa and a temperature of 900 °C, read from a type S thermocouple; the lower temperature allowed for a greater yield of the new phase relative to the bulk sample. This sample showed similar characteristics for the new phase in EPMA and powder X-ray diffraction to the results obtained in R-347. Subsequent experiments that attempted to isolate pure fluoride and hydroxide end-members of the compound were unsuccessful (Table 1), giving preliminary evidence that the compound is a hydroxyfluoride with no pure OH or F end-members.

Electron microprobe examination was performed using WDS with a JEOL 8600 microprobe, with a 10 nA beam current and an estimated 3 micrometer beam diameter. Element counts were standardized to MgF_2 (F), wollastonite (Ca), quartz (Si), and alumina (O). Ca and Si were analyzed with separate PET detectors, while O and F were analyzed with the same light-element detector.

A single crystal of the new phase approximately 40 micrometers in all dimensions was recovered from the polished probe mount of experiment R-347, and was mounted on a glass fiber for single-crystal X-ray diffraction. Diffraction patterns were obtained with a Bruker SMART APEX 2000, with Mo$K\alpha$ radiation, a graphite monochromator, and a 2000 K CCD detector. 3176 reflections from $h = -6$ to 6, $k = -12$ to 12, and $l = -7$ to 7 were collected. 712 independent reflections were included, of which 544 were listed as observed.

The single-crystal X-ray data were solved and refined using the program suite SHELX (Sheldrick 1997). Ionic structure factors were used for all atoms in the refinement (Ca^{2+}, Si^{4+}, O^{2-}, F^{-}). Determination of the possible locations of fluorine atoms was accomplished by allowing partially occupied F and O atoms to share the same site, with the constraints of both atoms having the same thermal parameters and coordinates and the total occupancy of the site to equal one (the site is fully occupied). The resulting refined occupancies of the sites clearly show the fluorine position (refined fluorine occupancy = 1.00), while the remaining possible positions refined to oxygen occupancy values ranging from 0.96 to 0.99. We therefore assigned a fully occupied F atom at the proper site and fully occupied O atoms at the other possible sites. Attempts were made to locate hydrogen atoms corresponding to the most reasonable peaks in the difference maps near the end of the refinement. Each attempt resulted in a worse fit to the data and unreasonable thermal parameters for the proposed hydrogen atom. This is presumably due to the small size of the crystal combined with the low scattering of the hydrogen atom. A final R_{obs} of 0.0623 and a goodness of fit of 1.103 were obtained. Further details of the structural refinement are listed in Table 2.

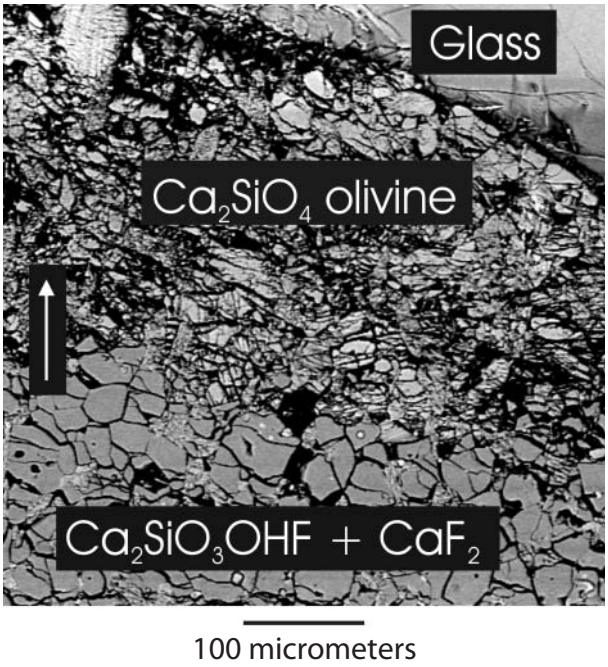

FIGURE 1. View of the sample from which the single crystals of Ca_2SiO_3OHF were recovered (R-347). The arrow shows the "up" direction during the run. The temperature also increases in the upward direction in the region shown; the calculated gradient across this area is about 50 °C. The layer of Ca_2SiO_3OHF + CaF_2 is below a layer of Ca_2SiO_4 olivine, while the capsule center and gravitational top of the capsule were filled with a transparent glass.

RESULTS AND DISCUSSION

Composition

Electron microprobe WDS analysis for Ca, Si, O, and F was used to measure the composition of the new phase. Some representative probe analyses are shown in Table 3. The new phase is beam-sensitive, and care had to be taken in the analysis. As both oxygen and fluorine were analyzed with the same detector, in alternating analyses either oxygen was measured first or fluorine was measured first. There was a systematic difference in the O and F contents depending on the order of oxygen and fluorine measurements, which is obvious in Table 3. About 20 reasonably good analyses points were obtained in sets with different standards and all the sets were consistent, but the set using wollastonite, corundum, and MgF_2 as standards gave the most reasonable totals and is used here as the primary compositional data. The first four of the five analyses were used to provide an even number of data in order to average the alternation in O and F quantities. The Ca, Si, and F contents are near a ratio of 2:1:1 in all the probe analyses, but the oxygen content is somewhat too high to be consistent with charge-balance. The raw probe data normalized to Ca indicate a composition of $Ca_{2.00}Si_{0.99}O_{4.39}F_{1.09}$. It appears that the oxygen measurement is high by about 0.4 units in this formula. Adjusting only the oxygen number to give the crystallographically derived cation to anion ratio results in a composition near the ideal midpoint composition between a pure OH end-member and a pure F end-member, i.e., nearly

TABLE 2. Summary of X-ray diffraction data for Ca_2SiO_3OHF

Crystal data	
Color	Colorless
Description	Block
Size (mm)	0.04 × 0.04 × 0.04
Crystal system	Monoclinic
Space group	$P2_1/c$
a	5.8111(7)
b	10.6050(13)
c	6.6968(8)
β	102.025(3)
V	403.65(8)
Z	2
Stoichiometric formula	H2 Ca4 F2 O8 Si2
Formula weight M_r	384.50
Calculated density (g/cm^3)	3.164
F(000)	388
Absorption coefficient μ(Mo) (mm^{-1})	3.044
Temperature (K)	293(2)
Reflections used for cell parameters	911
Cell measurement θ_{min}	5.26
Cell measurement θ_{max}	31.68
Data collection	
Radiation type	Mo*K*α
Radiation monochromator type	graphite
Diffractometer	Bruker SMART APEX
Measurement method	ω scan
Number of measured reflections	3176
Number of independent reflections	712
Number of observed reflections	544
Observed criterion	>2σ(*I*)
Absorption correction type	Empirical
No. frames collected:	1818
Frame width (w):	0.3°
Exposure time/frame:	120 s
Refinement	
Parameters refined	73
R_{all}	0.0915
R_{obs}	0.0623
wR_{all}	0.0921
wR_{obs}	0.0847
Goodness of fit (*S*)	1.103

TABLE 3. EPMA analyses of crystals from run R-347

	Ca	Si	O	F	Total
		Weight percents			
Analysis 1*	39.0	13.7	36.8	9.2	98.6
Analysis 2†	39.1	13.8	33.9	11.1	97.9
Analysis 3*	39.6	13.8	35.3	9.6	98.4
Analysis 4†	39.4	13.7	31.7	11.0	95.9
Weights	39.3(3)	13.8(1)	34.4(2.2)	10.2(1.0)	97.8(1.2)
Analysis 5*	39.6	13.7	35.6	9.1	98.0
		Atomic percents			
Analysis 1*	22.9	11.5	54.2	11.4	100
Analysis 2†	23.4	11.8	50.8	14.0	100
Analysis 3*	23.5	11.7	52.6	12.1	100
Analysis 4†	24.4	12.1	49.2	14.3	100
Weights	23.6(6)	11.8(2)	51.7(2.2)	12.9(1.4)	100
Analysis 5*	23.7	11.7	53.2	11.5	100

Notes: Probe current 10 nA, beam-sensitive crystals in the cold end of the capsule. Analyses 1, 3, and 5 were obtained with O first and F second on the light-element detector, analyses 2 and 4 with F first and O second. An even number of analyses was averaged in order to reduce bias from the alternation in O and F quantities. A crystal from the same sample was used for single-crystal X-ray diffraction.
* Oxygen was measured first.
† Fluorine was measured first.

TABLE 4. Atom positions from single-crystal X-ray diffraction, and bond valence sums (Brese and O'Keeffe 1991) calculated using the program Eutax (O'Keeffe, pers. comm.), for Ca_2SiO_3OHF

Atom	*x*	*y*	*z*	U_{iso}	bond valence sum
Ca1	0.2658(3)	0.0974(2)	0.0454(2)	0.0067(4)	2.007
Ca2	0.1886(3)	0.6976(2)	0.1925(3)	0.0071(4)	1.910
Si	0.3138(4)	0.3855(2)	0.0988(3)	0.0059(5)	4.013
O1	0.3902(9)	0.4976(5)	0.2570(7)	0.0090(13)	1.988
O2	0.5193(9)	0.2932(5)	0.0557(7)	0.0121(14)	1.758
O3	0.1110(9)	0.3027(5)	0.1621(8)	0.0153(14)	1.858
OH1	0.1705(9)	0.4481(5)	–0.1258(8)	0.0118(14)	1.313
F1	0.1404(7)	0.8909(4)	0.0281(6)	0.0105(11)	1.013

Note: The site occupancy factors are all 1.0.
SG $P2_1/c$; a = 5.8111(7), b = 10.6050(13), and c = 6.6968(8) Å, β = 102.025(3)°; V = 403.65 Å^3, Z = 4.

TABLE 5. Anisotropic displacement parameters (Å^2)

Atom	U_{11}	U_{22}	U_{33}	U_{23}	U_{13}	U_{12}
Ca1	0.0066(9)	0.0048(9)	0.0085(9)	–0.0011(8)	0.0012(7)	–0.0006(7)
Ca2	0.0060(9)	0.0072(9)	0.0081(9)	0.0003(8)	0.0014(7)	0.0014(8)
Si1	0.0068(12)	0.0063(13)	0.0046(11)	0.0009(10)	0.0008(9)	–0.0011(10)
O1	0.013(3)	0.009(3)	0.004(3)	0.001(3)	0.002(2)	0.002(3)
O2	0.012(3)	0.018(4)	0.007(3)	0.001(3)	0.003(2)	0.001(3)
O3	0.019(3)	0.011(3)	0.017(3)	–0.001(3)	0.006(3)	–0.001(3)
OH1	0.011(3)	0.014(3)	0.009(3)	–0.004(3)	0.000(3)	0.003(3)
F1	0.011(2)	0.009(3)	0.014(2)	–0.001(2)	0.006(2)	–0.002(2)

Ca_2SiO_3OHF. The H content in this ideal composition is expected to be 0.53 wt%, leading to an ideal total of 99.5 wt% for Ca, Si, O, and F. The somewhat lower average total near 98 wt% is typical of hydrogen-bearing minerals analyzed in the microprobe. Although experiments were performed to try to make either an OH or an F end-member of this phase (Table 1), they were not found. From this observation, combined with the microprobe results, it is tentatively concluded that this is a "line phase" which is most stable for the 50/50 composition between $Ca_2SiO_3(OH)_2$ and $Ca_2SiO_3F_2$, i.e., the composition Ca_2SiO_3OHF.

Structure

The structural information and bond valence sums from single-crystal X-ray diffraction are shown in Table 4. Anisotropic thermal parameters for all the atoms refined are presented in Table 5. There are two eight-coordinated Ca sites, one tetrahedral Si site, and five anion sites. From the composition data and charge balance, two of the anion sites are expected to host OH and F. Two of the sites, anion sites 4 and 5, are highly underbonded when they are occupied by oxygen, with bond-valence sums of 1.31 and 1.42, respectively, well below the ideal value of 2.00. When fluorine is placed at the sites instead, the bond valence sums are 1.01 and 1.08, close to the ideal value of 1.00. These two sites are likely locations for F and OH. One of these sites is bonded to the Si atom; the other site is the only anion site in the structure that is not bonded to the Si atom. A search of the ICSD database (Berndt 1997) reveals that no examples of crystalline compounds with SiO_3F tetrahedra have been reported, whereas examples of structures with SiO_3OH tetrahedra are numerous.

A refinement of O vs. F for all of the sites, described further in the experimental section, indicates that the one anion site that is bonded only to calcium is fully occupied by fluorine, whereas the other four are fully occupied by oxygen. This gives a composition for the phase that is consistent with the probe composition, having an Si/F ratio of 1.0 and a Ca/F ratio of 2.0. This assignment is also quite consistent with the crystal chemical arguments. These factors together lead to the assignments of O,

TABLE 6. Selected bond lengths (in Å), and bond valences (calculated using the program Eutax (O'Keeffe, pers. comm.) for Ca_2SiO_3OHF

Ca1	-O1	2.401(5)	0.309
		2.419(5)	0.295
	-O2	2.538(6)	0.213
	-O3	2.540(6)	0.212
		2.749(5)	0.121
	-OH1	2.428(5)	0.287
	-F1	2.303(4)	0.287
		2.312(5)	0.281
Ca2	-O1	2.418(5)	0.296
	-O2	2.358(5)	0.348
		2.613(5)	0.174
	-O3	2.435(5)	0.282
		2.636(5)	0.164
	- OH1	2.560(5)	0.201
	-F1	2.317(5)	0.278
		2.504(4)	0.167
Si	-O1	1.593(6)	1.088
	-O2	1.616(6)	1.022
	-O3	1.596(6)	1.078
	-OH1	1.696(5)	0.824

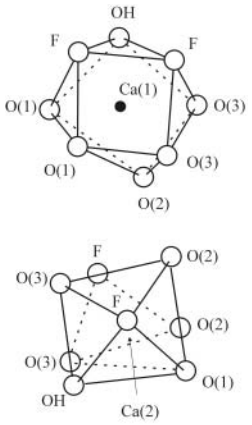

FIGURE 2. Coordination polyhedra around calcium atoms. (**a**) Ca1 (square antiprism). (**b**) Ca2 (triangle overlain by a monocapped square/square pyramid). The Ca2 atom is hidden behind the capping F atom of the polyhedron.

OH, and F given in Table 4. The unambiguious assignment of the sites helps to simplify the discussion of the structure; however, it should be emphasized that optical spectroscopic and NMR data are needed to better characterize the distribution of OH and F in this compound.

A table of bond lengths is given in Table 6. The two eight-coordinated calcium sites, Ca1 and Ca2, are both centers of polyhedra represented by the composition CaO_5OHF_2. These coordination polyhedra are shown in Figure 2. One of the calcium atoms, Ca1, forms a fairly regular square antiprism, and the other, Ca2, a more irregular 1-4-3 figure (i.e., a triangle overlain by a monocapped square, or square pyramid). This looks similar to the 4–3 polyhedron in monoclinic zirconia, or high-pressure $Ca(OH)_2$, but with the square face capped. The high coordination of the calcium atoms is characteristic of the effect of pressure. By comparison, the fluoride end-member of the mineral cuspidine, $Ca_4Si_2O_7F_2$, the only known compound combining CaO, SiO_2, and CaF_2, has calcium in six-coordination.

The packing of the calcium polyhedra is quite complex. The structure is not based on close-packing of neighbors or next-nearest neighbors, in contrast to the ccp and hcp packing of many high-pressure oxides and silicates. Figure 3 shows a general view of the structure looking down **a**. There is face-sharing between some of the Ca polyhedra: a series of Ca2 polyhedra that form face-sharing chains along **c** can be seen running from left to right in Figure 3. Each polyhedron shares faces with two mirror image polyhedra. The faces shared are one of the four top faces of the square pyramid (the F-O3-O2 face) and the triangular base (see Fig. 2). The calcium polyhedra also link by edge-sharing between Ca1 and Ca1 and between Ca1 and Ca2 polyhedra.

A prominent structural feature, visible in Figure 3, is the presence of narrow channels along **a**; these channels contain the SiO_3OH tetrahedra in alternating pairs. The centers of the channels lie along the symmetry-equivalent lines (x, 0.5, 0) and (x, 0, 0.5). These lines are arranged in a nearly hexagonal fashion. The approximately hexagonal array lies in the plane of **b** and $\mathbf{c}_p$, where $\mathbf{c}_p$ is the projection of the **c**-axis onto **c*** [$\mathbf{c}_p$ = **c**cos(90-β); Hahn 1992]. If the array were exactly hexagonal,

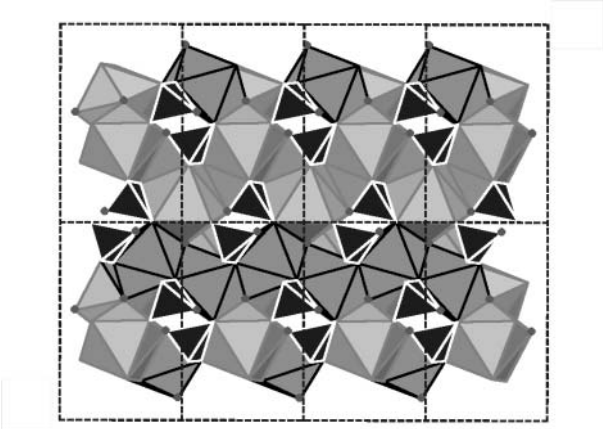

FIGURE 3. A general view of the structure of Ca_2SiO_3OHF, viewed along [100]. The **b**-axis is down the page, $\mathbf{c}_p$ is to the right. The SiO_4 tetrahedra are shown in black; the Ca1 polyhedra are lightly shaded, and the Ca2 polyhedra are slightly darker with thicker outlines. One face-sharing chain of Ca2 polyhedra runs horizontally, along **c**, about 2/3 of the way down the diagram. The fluorine and hydroxyl ions are shown as small spheres; the O ions are not shown. The SiO_4-containing channels, with the channel centers forming a nearly hexagonal array, is most clearly visible in this projection. The orientations of the tetrahedra alternate along the channel axis.

the ratio $\mathbf{b}/\mathbf{c}_p$ would be equal to $\sqrt{3}/3$, or 0.577. In Ca_2SiO_3OHF, the ratio $\mathbf{b}/\mathbf{c}_p$ is equal to 0.618, which is distorted by 7.1% from the ideal value. The distortion elongates the hexagonal array in the **b**-direction. The hexagonal arrangement of the channels may lead to stabilization of the structure; hexagonal arrays of either atoms or voids are a common feature of crystals. In the current case, the hexagonal arrangement of channels contrasts strongly with the atomic arrangement itself, which departs markedly from hexagonal symmetry.

The walls of the channels are formed by rings of CaO_5OHF_2 polyhedra. There are five polyhedra in the **b**-**c** plane for which the calcium atoms are approximately coplanar. These share edges with a staggered set of five more polyhedra in the next layer

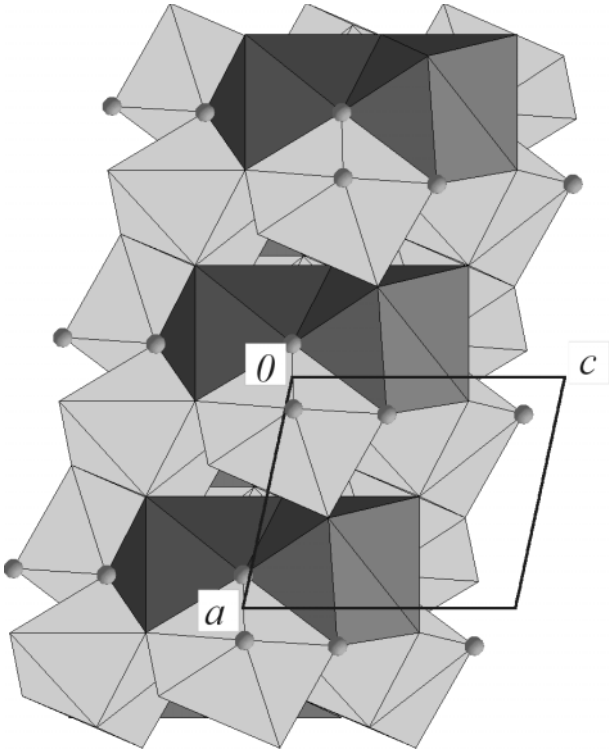

FIGURE 4. A projection on (010) of one of the columns of CaO_5OHF_2 polyhedra surrounding the structural channel in the Ca_2SiO_3OHF structure. The **c**-axis is to the right in the picture, and the column axis is parallel to **a**. The Si tetrahedra have been removed from the drawing; the Ca1 polyhedra are shown lighter and the Ca2 polyhedra are shown darker.

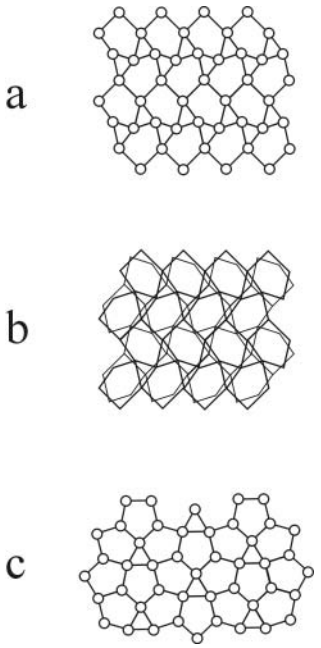

FIGURE 5. (**a**) View of the calcium net (one layer) in Ca_2SiO_3OHF, projected along **a**. The $\mathbf{c}_p$ axis is horizontal and the **b** axis is vertical in this drawing. The locations of the Ca atoms are represented by the open circles. (**b**) Superimposed nets from the two symmetrically identical, overlain Ca layers (Ca atoms not shown), same projection as in Figure 5a. The top layer is shown by thicker lines, the bottom layer by thinner lines. (**c**) The α-U_3O_8 net O'Keefe and Hyde, 1996, p. 172), which is another net containing 3-sided and 5-sided units.

below, forming an alternating ring of 10 polyhedra. A side view of the polyhedral wall of a channel is shown in Figure 4.

A separate aspect of the structure may be seen by examining the locations of calcium atoms alone. The calcium atoms lie in approximately planar nets lying in the **b**-**c** plane. In the calcium net, five-rings and three-rings coexist (Fig. 5a) in the sequence 5-3-5-3. The net alternates with its inverted image along **a** to define the wall of the channel, as shown in Figure 5b. The five-rings, although distorted significantly from a pentagonal shape and looking more like a square with a triangular cap, are nonetheless a natural physical choice for defining the net, because the rings physically surround the channels in the structure. The calcium net in this structure can be compared to the α-U_3O_8 net (Fig. 5c) (O'Keeffe and Hyde 1996, p. 172) that also has 5-rings and 3-rings, but in the sequence 5-5-5-3.

Fluorine and hydroxyl ions

As was mentioned above, the SiO_3F group has not, to our knowledge, been reported in any structural studies of crystalline compounds. Four apparent examples from the ICSD database (Fluck 1996) turned out to all contain only SiO_4 tetrahedra according to the original references (Brown 1978; Mazzi et al. 1979; Canillo et al. 1992; Oberti et al. 1997), and the presence of Si-F bonds in the search appears to be due to misprints in the database in all four cases. However, not only SiO_3F units but also SiO_2F_2 units occur in fluorine-doped silica glass, according to the results of NMR spectroscopy (Duncan et al. 1986). SiO_3F groups were also inferred from IR data on a series of fluorine-incorporated amorphous films by Kim et al. (2001), who observed a frequency increase in the Si-O stretching vibration and the appearance of an Si-F stretching mode as F was added to SiO_2 films. In contrast, in binary silicate glasses and ternary aluminosilicates with small amounts (1 wt%) of fluorine, there is a strong trend against Si-F bonding, with only the sodium silicate glasses exhibiting a measurable Si-F bonding component in NMR spectra (Stebbins et al. 2002). Thus there is some possibility that fluorine can be part of the silica tetrahedron, and optical spectroscopy and NMR studies of Ca_2SiO_3OHF and other fluorine-bearing silicates would help to clarify this, and it would be interesting to compare them to the glass structures previously studied by these techniques.

The H atoms could not be located in the data due to the small size of the crystal; however, there is a shorter OH-O1 distance of 2.925 Å that could accommodate a hydrogen bond. This hydrogen bonding would also raise the bond sum to O1. There are also similar short distances for F-O1, allowing the possibility that some OH could be at that site and bonding to O1.

The low stability of the SiO3F group should limit the solubility of fluorine in the hypothetical solid solution $Ca_2SiO_3(OH,F)_2$. Any composition with an F content of 50% or lower does not require F to bond to the Si atom, but any further increase in F content requires it. If OH can go into the fluorine site, there could be a solid solution toward the OH-rich side.

TABLE 7. Angles for the Si tetrahedron in Ca_2SiO_3OHF

O3-Si-OH1	101.4(3)
O1-Si-OH1	108.4(3)
O3-Si-O2	109.2(3)
O2-Si-OH1	108.9(3)
O1-Si-O3	110.7(3)
O1-Si-O2	117.2(3)

The termination of a tetrahedron by an OH group should lead to reduced structural polymerization, because the Si-OH tetrahedral bond leads to near saturation of the hydroxyl ion and thus does not bridge to other structural units. In the current case, the Si-OH bond does not fully terminate the tetrahedron; the valence of the bond is 0.82, whereas a value of 1.00 would indicate saturation. The hydroxyl group at OH1 is instead weakly bonded to two calcium atoms. Possibly as a result of the association with the calcium atoms, the Si-OH bond length in Ca_2SiO_3OHF is slightly elongated, to 1.697 Å.

The four distances and six angles in the tetrahedron are shown in Tables 6 and 7. The primary distortion of the tetrahedron is through the displacement of one oxygen atom toward the OH atom, shown by the O3-Si-OH angle of 101.4°. This is compensated for by an expansion of the opposite angle in the tetrahedron, with an O1-Si-O2 angle of 117.2°. The rest of the O-Si-O and O-Si-OH angles are near the theoretical value of close to 109.5°. For a free $SiO_3(OH)$ unit, the distortion of the tetrahedron would follow the symmetry of the atom placements on the tetrahedron, point group 3*m*; the result would be an umbrella-like displacement of all 3 O atoms toward the hydroxyl group. The observed tetrahedron is close in topology to the point group *m*, with the mirror plane passing through Si, OH1, and O3 (although it is not a true mirror because O1 and O2 are not symmetrically equivalent). The lowered symmetry of the distortion is not surprising given the complex surroundings of the SiO_3OH group in this particular compound.

Stability of the Ca_2SiO_3OHF phase

Although not providing dense enough coverage for detailed phase equilibria, the series of experiments performed for this study can give some information about the stability of Ca_2SiO_3OHF. A micrograph from the experiment from which the crystals for this study were taken is shown in Figure 1 (R-347). The solid parts of the experimental product consists of three layers. A layer of the new phase Ca_2SiO_3OHF coexisting with CaF_2 in the fluorite structure is located at the end of the capsule nearest the thermocouple; this end was gravitationally downward. A layer of pure Ca_2SiO_4 olivine is found further into the capsule. The center and gravitational top of the capsule are filled with a transparent glass interpreted to be a quenched melt. Similar textures and layering were seen in all of the experiments in the system. Also, in some of the H_2O-bearing samples, voids were found near the top of the capsule that may have been formed by an H_2O-rich phase immiscible in the melt.

The layering may be interpreted in terms of thermal gradient effects in the sample, combined with gravitational settling of the solids. The thermal gradient across the sample for this assembly has been calculated using a finite-difference algorithm (Hernlund et al. 2000). The calculation indicates that when the thermocouple reads 1100 °C, the temperature ranges from 1115 °C at the point inside the Pt capsule closest to the thermocouple to 1220 °C at the hottest location in the capsule, which is along the circle around the outside center or "equator" of the capsule, in the center plane of the furnace. Thus the thermal gradient within the sample is about 105 °C for the conditions used in these syntheses. None of the experimental products contain any Ca_2SiO_3OHF above about 1130 °C, which gives a minimum estimate for the limit of thermal stability of this phase at 8 to 9 GPa (the actual stability limit for the ideal bulk composition in the absence of a thermal gradient could be higher than this but not lower).

The texture further establishes that Ca_2SiO_4 is a liquidus phase (since it is in direct contact with the liquid), and the Ca_2SiO_3OHF and expanded fluorite coexist at lower temperatures. Unfortunately, the glasses were difficult or impossible to analyze because of extreme beam sensitivity in the electron microprobe. Because of this and the thermal gradient and chemical separation during the run, including the strong segregation of H_2O to the top of the capsule, care should be taken in interpreting phase relations from these data beyond these broad inferences. The liquid is possibly very H_2O-rich but is an excellent glass-former, a common observation in various calcium-rich silicate systems (cf. Irving et al. 1977).

ACKNOWLEDGMENTS

The targeted synthesis, crystal structure determination, and microprobe studies were carried out with the support of NSF EAR-0074089 to K. Leinenweber. The authors acknowledge J. Holloway for providing many starting materials and capsule-sealing equipment and advice. M. O'Keefe is thanked for inspirations on structural interpretation. Thanks to J. Stebbins for pointing out the NMR work on fluorine in silicate glasses. G. Moore provided training and expertise on the electron microprobe. K. Ekbundit and C. Bonneau helped with graphics. The manuscript benefited greatly from careful reviews by W. Crichton and P.F. Zanazzi.

REFERENCES CITED

Angel, R.J. (1997) Transformation of fivefold-coordinated silicon to octahedral silicon in calcium silicate, $CaSi_2O_5$. American Mineralogist, 82, 836–839.

Angel, R.J., Ross, N.L., Seifert, F., and Flierveot, T.F. (1996) Structural characterization of pentacoordinate silicon in a calcium silicate. Nature, 384, 441–444.

Berndt, M. (1997) ICSD/RETRIEVE 2.01 Crystal Structure Database. Gmelin Institute/FIZ Karlsruhe, Germany.

Brese, N.E. and O'Keeffe, M. (1991) Bond-valence parameters for solids. Acta Crystallographica, B47, 192–197.

Brown, B.E. (1978) The crystal structure of a 3*T* lepidolite. American Mineralogist, 63, 332–336.

Cannillo, E., Giuseppetti, G., Mazzi, F., and Tazzoli, V. (1992) The crystal structure of a rare earth bearing leucophanite: $(Ca,RE)CaNa_2Be_2Si_4O_{12}(F,O)_2$. Zeitschrift für Kristallographie, 202, 71–79.

Dai, Y. and Post, J.E. (1995) Crystal structure of hillibrandite: A natural analogue of calcium silicate hydrate (CSH) phases in Portland cement. American Mineralogist, 80, 841–844.

Duncan, T.M.; Douglass, D.C., Csencsits, R., and Walker, K.L. (1986) Study of fluorine in silicate glass with ^{19}F nuclear magnetic resonance spectroscopy. Journal of Applied Physics, 60, 130–136.

Fluck, E. (1996) Inorganic Crystal Structure Database (ICSD) and Standardized Data and Crystal Chemical Characterization of Inorganic Structure Types (TYPEIX)—Two tools for inorganic chemists and crystallographers. Journal of Research of the National Institute of Standards and Technology, 101, 217–220.

Hahn, T., ed. (1992) International Tables for Crystallography. Kluwer Academic Publishers, Dordrecht.

Hernlund, J.W., Locke, D.R., Leinenweber, K.D., and Tyburczy, J.A. (2000) Numerical model of temperature distribution in the multiple anvil device. Eos, Transactions of the American Geophysical Union, 81, F1299.

Holloway, J.R., Pan, V., and Gudmundsson, G. (1992) High-pressure fluid-absent melting experiments in the presence of graphite—oxygen fugacity, ferric-ferrous ratio and dissolved CO_2. European Journal of Mineralogy, 4, 105–114.

Irving, A.J., Huang, W.-L., and Wyllie, P.J. (1977) Phase relations of portlandite, $Ca(OH)_2$ and brucite, $Mg(OH)_2$ to 33 kilobars. American Journal of Science, 277, 313–321.

Kim, Y., Hwang, M.S., Kim, H.J., Kim, J.Y., and Lee, Y. (2001) Infrared spectroscopic study of low-dielectric-constant fluorine-incorporated and carbon-incor-

porated silicon oxide films. Journal of Applied Physics, 90, 3367–3370.
Koller, H., Wölker, A., Villaescusa, L.A., Díaz-Cabañas, M.J., Valencia, S., and Camblor, M.A. (1999) Five-coordinate silicon in high-silica zeolites. Journal of the American Chemical Society, 121, 3368–3376.
Leinenweber, K. and Parise, J. (1995) High-pressure synthesis and crystal structure of $CaFeTi_2O_6$, a new perovskite structure type. Journal of Solid State Chemistry, 114, 277–281.
Marsh, R.E. (1994) A revised structure for α-dicalcium silicate hydrate. Acta Crystallographica, C50, 996–997.
Mazzi, F., Ungaretti, L., Dal Negro, A., Peterson, O.V., and Rönsbo, J.G. (1979) The crystal structure of semenovite. American Mineralogist, 64, 202–210.
Morris, E., Groy, T., and Leinenweber, K. (2001) Crystal structure and bonding in the high-pressure form of fluorite (CaF_2). Journal of Physics and Chemistry of Solids, 62, 1117–1122.
Oberti, R., Hawthorne, F.C., and Raudsepp, M. (1997) The behaviour of Mn in amphiboles: Mn in synthetic fluor-edenite and synthetic fluor-pargasite. European Journal of Mineralogy, 9, 115–122.
O'Keeffe, M. and Hyde, B.G. (1996) Crystal Structures I. Patterns and Symmetry. Monograph 3, Mineralogical Society of America, Washington, D.C.
Ringwood, A.E. and Major, A. (1971) Synthesis of majorite and other high pressure garnets and perovskites. Earth and Planetary Science Letters, 12, 411–418.
Saburi, S., Kawahara, A., Henmi, C., Kusachi, I., and Kihara, K. (1977) The refinement of the crystal structure of cuspidine. Mineralogical Journal, 8, 286–298.
Sheldrick, G.M. (1977) SHELXTL PC, Version 5.1, An Integrated System for Solving, Refining, and Displaying Crystal Structures from Diffraction Data. Bruker Analytical X-Ray Instruments, Inc. Madison, Wisconsin, U.S.A.
Stade, H., Heidemann, D., and Wallis, B. (1998) Neue verbindungen im system $CaO/SiO_2/CaCl_2/H_2O$. Zeitschrift für anorganische und allgemeine Chemie, 624, 1551–1557.
Stebbins, J.F. and Poe, B.T. (1999) Pentacoordinate silicon in high-pressure crystalline and glassy phases of calcium disilicate ($CaSi_2O_5$). Geophysical Research Letters, 26, 2521–2523.
Stebbins, J.F., Sandland, T.O., Du, L.-S., and Kiczenski, T.J. (2002) Structural environments for chloride and fluoride ions in aluminosilicate glasses: NMR results. Geochemica et Cosmochemica Acta, 66, A736–A736.
Walker, D. (1991) Lubrication, gasketing, and precision in multianvil experiments. American Mineralogist, 76, 1092–1100.
Xu, H. and Buseck, P.R. (1996) TEM investigation of the domain structure and superstructure in hillebrandite, $Ca_2SiO_3(OH)_2$. American Mineralogist, 81, 1371–1374.
Yano, T., Urabe, K., Ikawa, H., Teraushi, T., Ishizawa, N., and Udagawa, S. (1993) Structure of α-dicalcium silicate hydrate. Acta Crystallographica, C49, 1555–1559.

MANUSCRIPT RECEIVED OCTOBER 23, 2003
MANUSCRIPT ACCEPTED JUNE 13, 2004
MANUSCRIPT HANDLED BY ALISON PAWLEY